Monitoring forests using SAR images

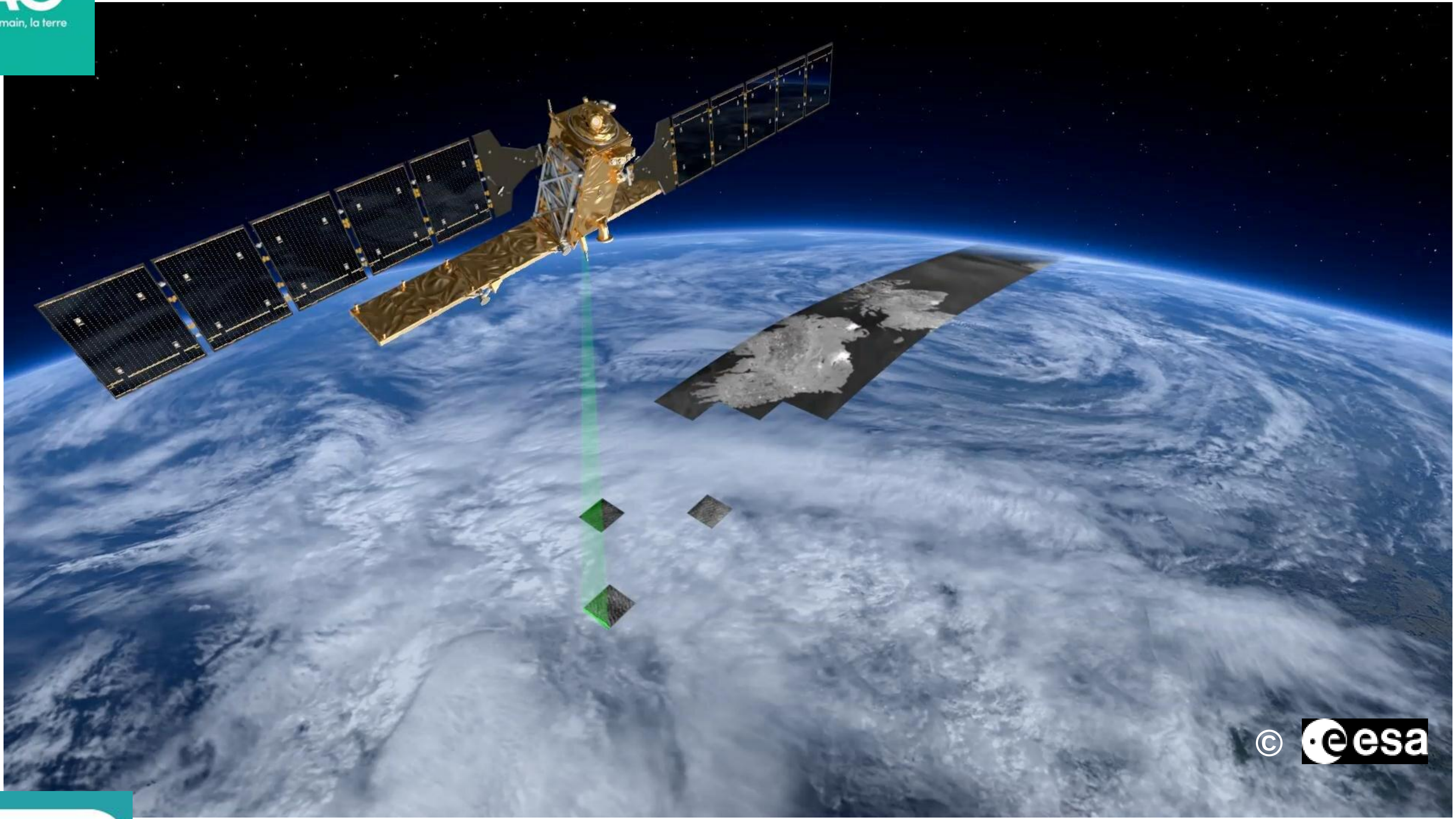

Frédéric Frappart
frederic.frappart@inrae.fr

Outline

- ❖ Introduction
- ❖ Forest cover mapping
- ❖ Forest stand height estimation

Introduction

Forests in Europe and contribution to global carbon cycle

- Forests cover 33% of Europe’s total land area
- European forests area ~ 2.15 M km^2
  and growing stock ~ 35 billion m^3
- Forests area and growing stock continue to increase since 1990
- Increase of the growing stock larger than world’s average
- Forests absorb 9% of the total GHG emissions in Europe
- Carbon stored in different tree compartments
  mostly in forest soil
- Carbon stocks and changes by forests crucial for climate
  change mitigation and adaptation
  e.g., EU Forest strategy 2030

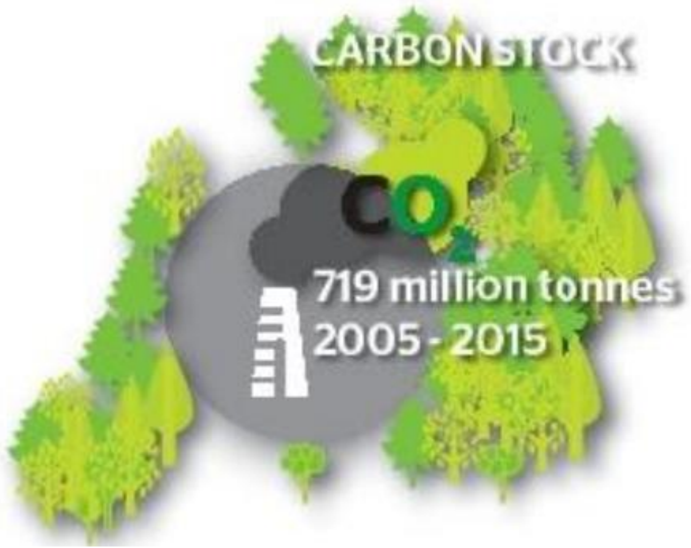

State of Europe’s Forests (2015)

Forests in Europe and contribution to global carbon cycle

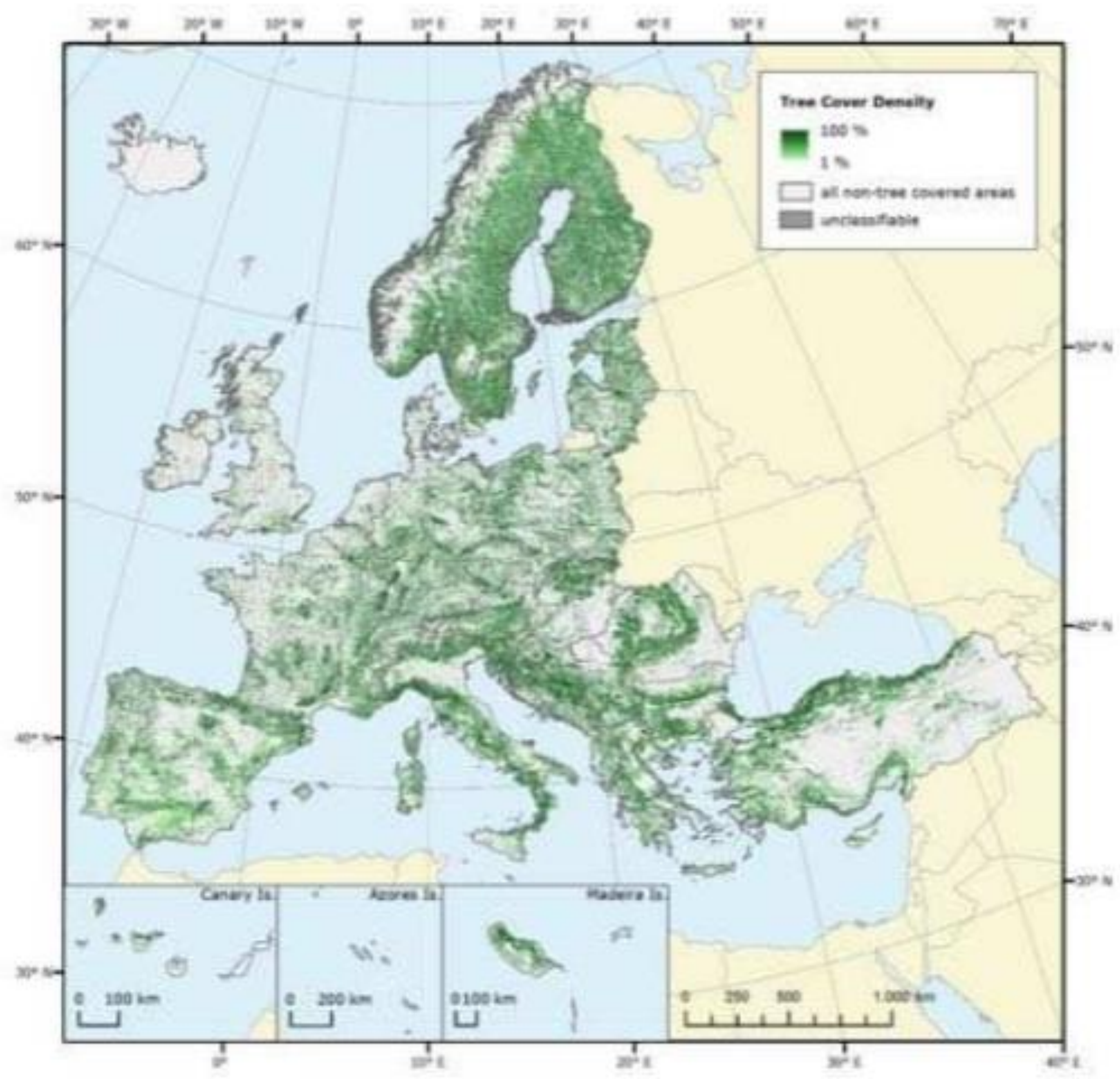

2015 Pan-European tree cover
Copernicus Programme

Forest health in Europe

- **In Europe, over 1950-2019: 43.8 million m3 of wood damaged annually by natural disturbances**

  - Storms (46%)

  - Fires (24%) Patacca et al. (2023)

  - Bark beetles (17%) but doubled during the last 20 years

- **Abiotic damage (e.g., droughts or storms) may not only be directly harmful**
  but also contribute to the increase in biotic damage in subsequent years through:

  - the deterioration of tree conditions

  - the increase in their susceptibility to pests.

- **And conversely (Stephens et al., 2018)**

Forest health in Europe

- ~3.1% (37,000 km²) of Europe's forests affected by damage caused by biotic/abiotic factors

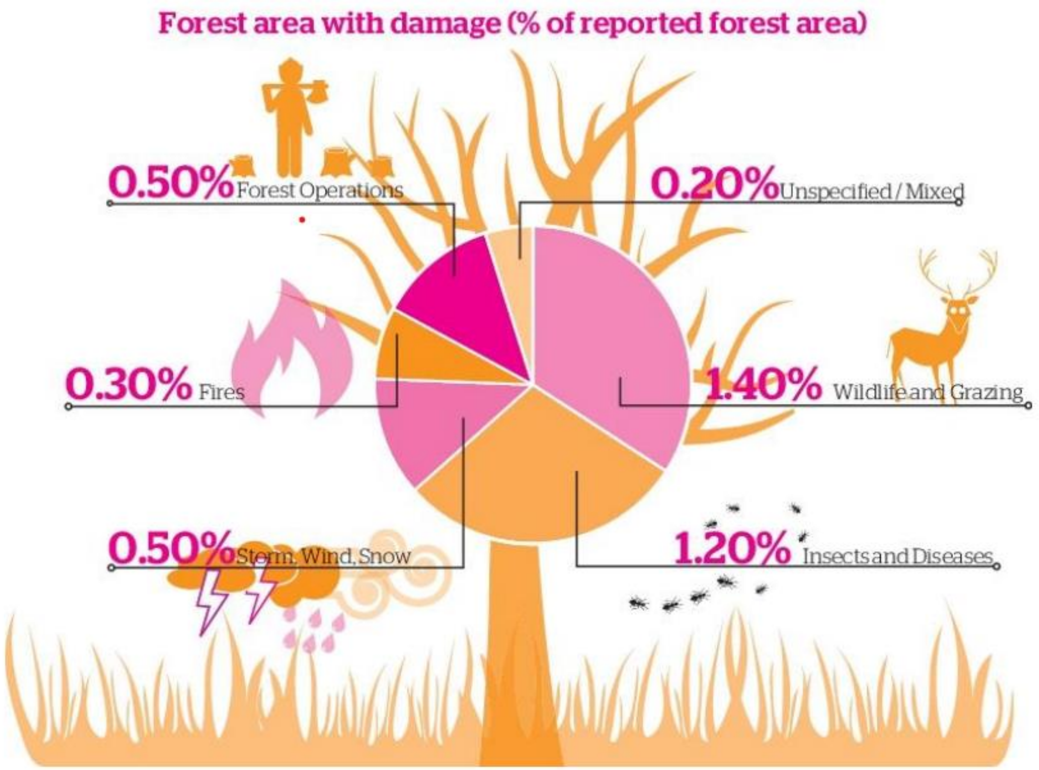

State of Europe's Forests (2015)

- Damages caused by pests affect a much higher area than forest fires in Europe

Interest of radar images

❖ **Independence of solar illumination**

⇒ can be acquired night and day

❖ **Independence of weather conditions**

⇒ much longer wavelengths than optical or IR microwaves easily penetrate clouds

Presence of convective raincells can be observed on images acquired at C and X bands

Example: Two Sentinel-1 (C-band) from 20/10/2018 (left) and 13/11/2018 (right) displayed in RGB: VV, VH, NDI(VV,VH) over Congo

Ygorra et al. (2021). Monitoring loss of tropical forest cover from Sentinel-1 time-series. *International Journal of Applied Earth Observation and Geoinformation*, *103*, 102532.

View of Udinese (Italy) from

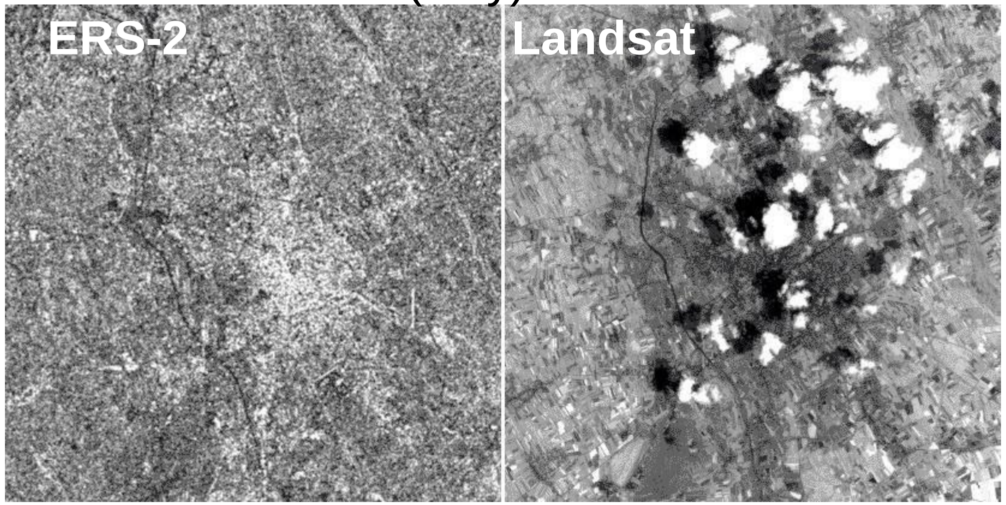

https://earth.esa.int/eogateway/missions/ers/radar-courses/radar-course-2

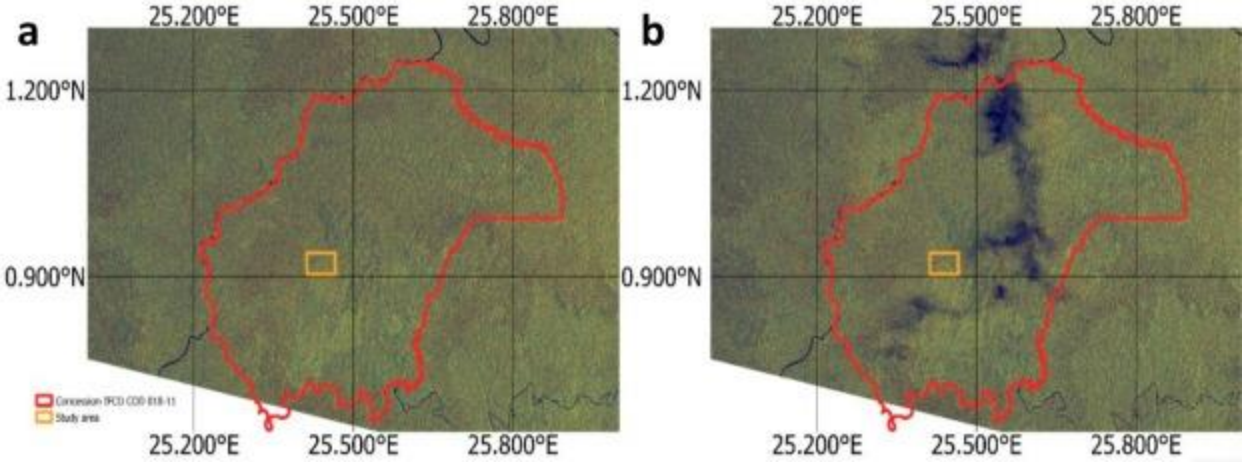

Forest cover mapping

SAR characteristics for forest mapping

SAR backscattering

❖ Sensor characteristics :

- wavelength (P, L, C, X)

- polarisation (HH, HV, VH, VV)

- incidence angle

❖ Target characteristics :

- roughness (soil, vegetation, both)

- soil and vegetation moisture

- vegetation density

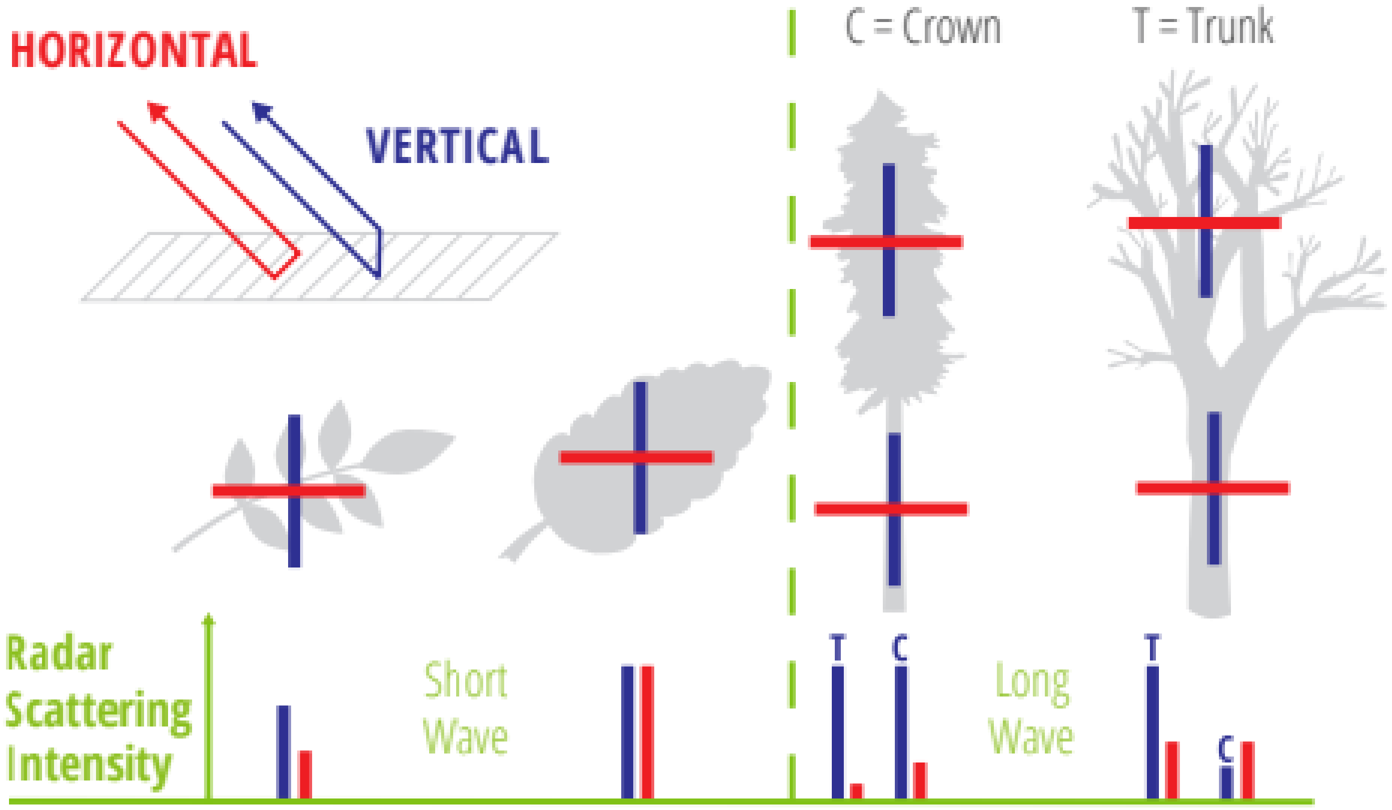

Schematic efects of polarization
on backscatter of long and short wavelengths
scattering from trunks and crowns
(Flores et al., 2019)
https://ntrs.nasa.gov/api/citations/20190002563/downloads/20190002563.pdf

Wavelength and polarisation for forest mapping

❖ Napo River, Amazonia (Flores et al., 2019)

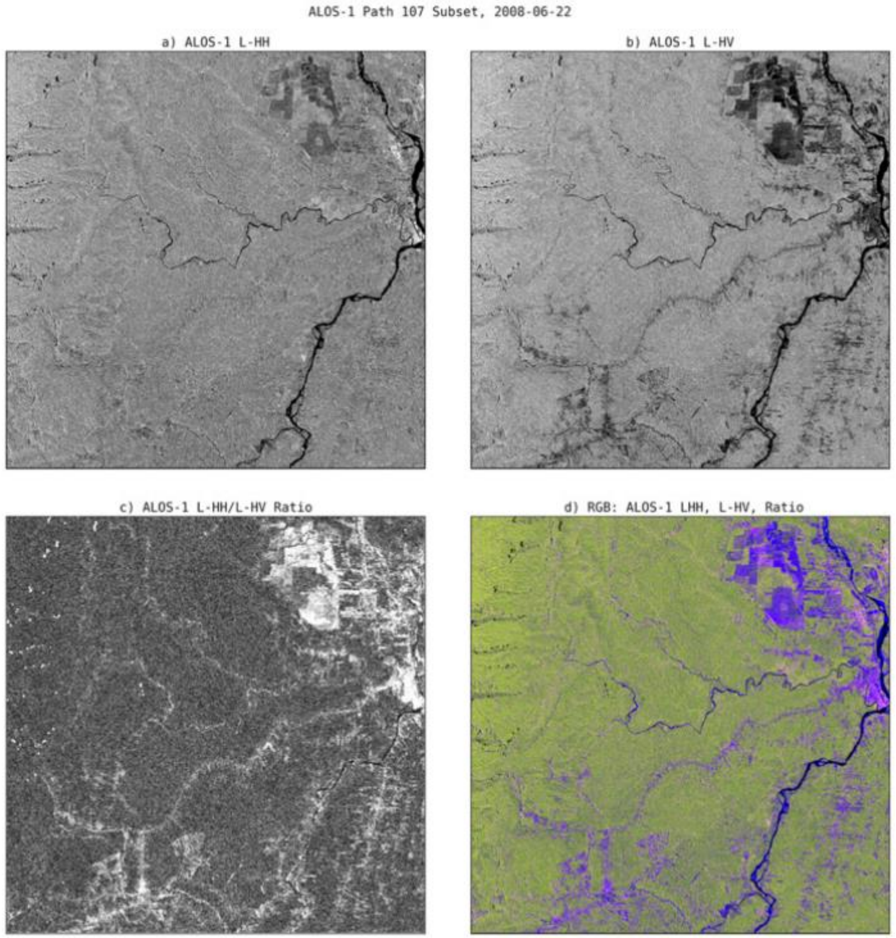

ALOS-1 L-band images: (a) L-HH, (b) L-HV, (c) ratio, and (d) RGB composite LHH/LHV/ratio (22/06/2008).

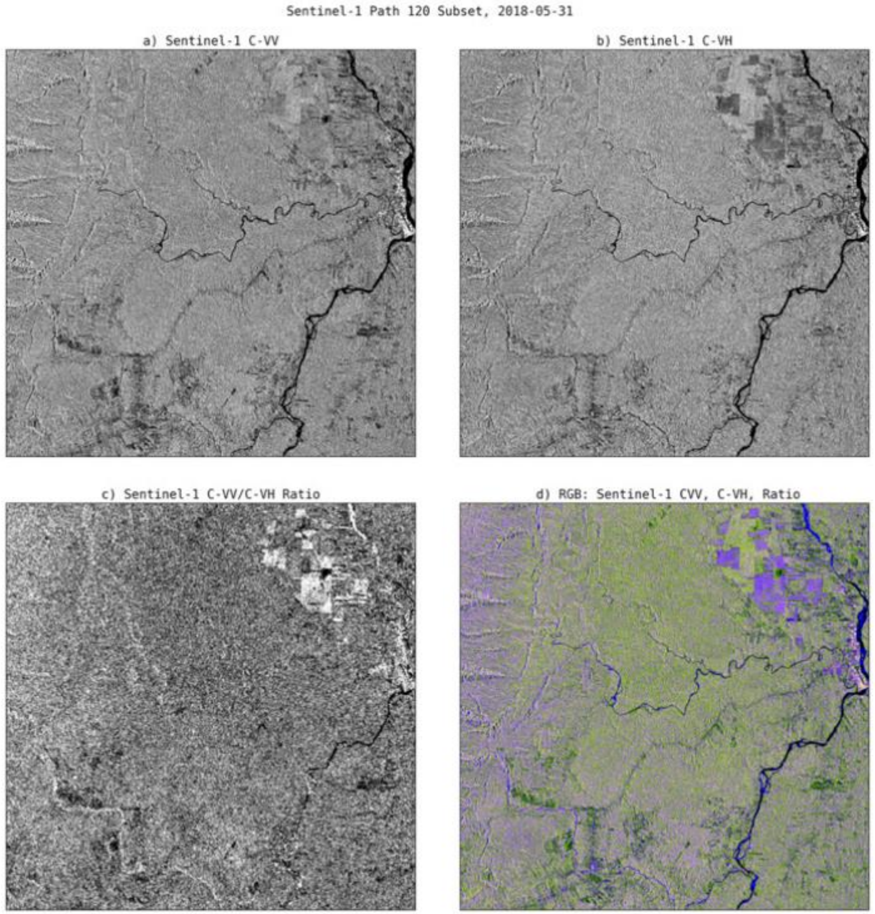

Sentinel-1 C-band images: (a) C-VV, (b) C-VH, (c) ratio, and (d) RGB composite CVV/CVH/ratio (31/05/2018)

Effect of the incidence angle

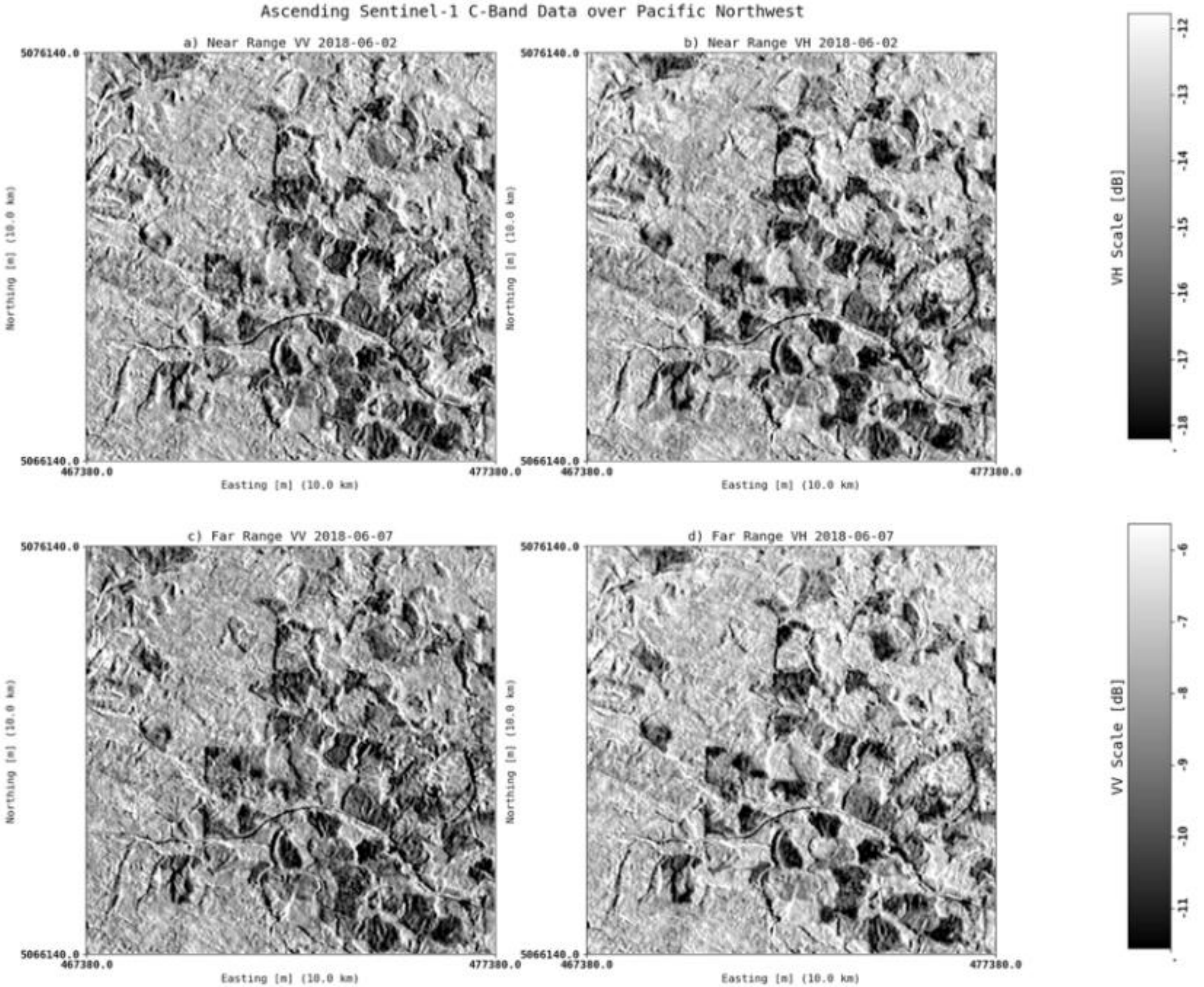

Near- and far-range acquisitions of Sentinel-1 CVV and CVH data over a forested site in the Pacifc Northwest.

(Flores et al., 2019)

Effect of the incidence angle

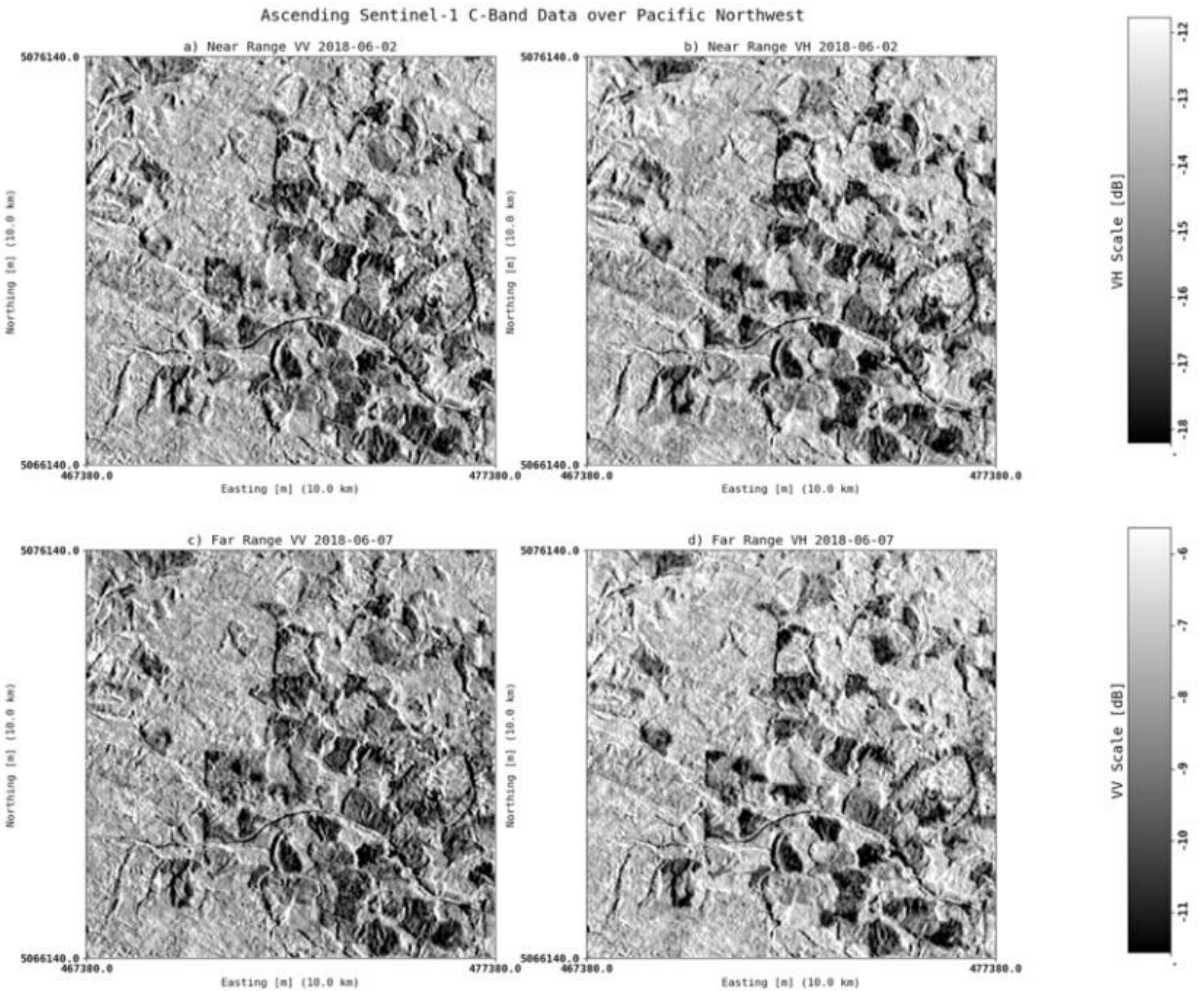

Near- and far-range acquisitions of Sentinel-1 CVV and CVH data over a forested site in the Pacifc Northwest.

(Flores et al., 2019)

Effect of moisture

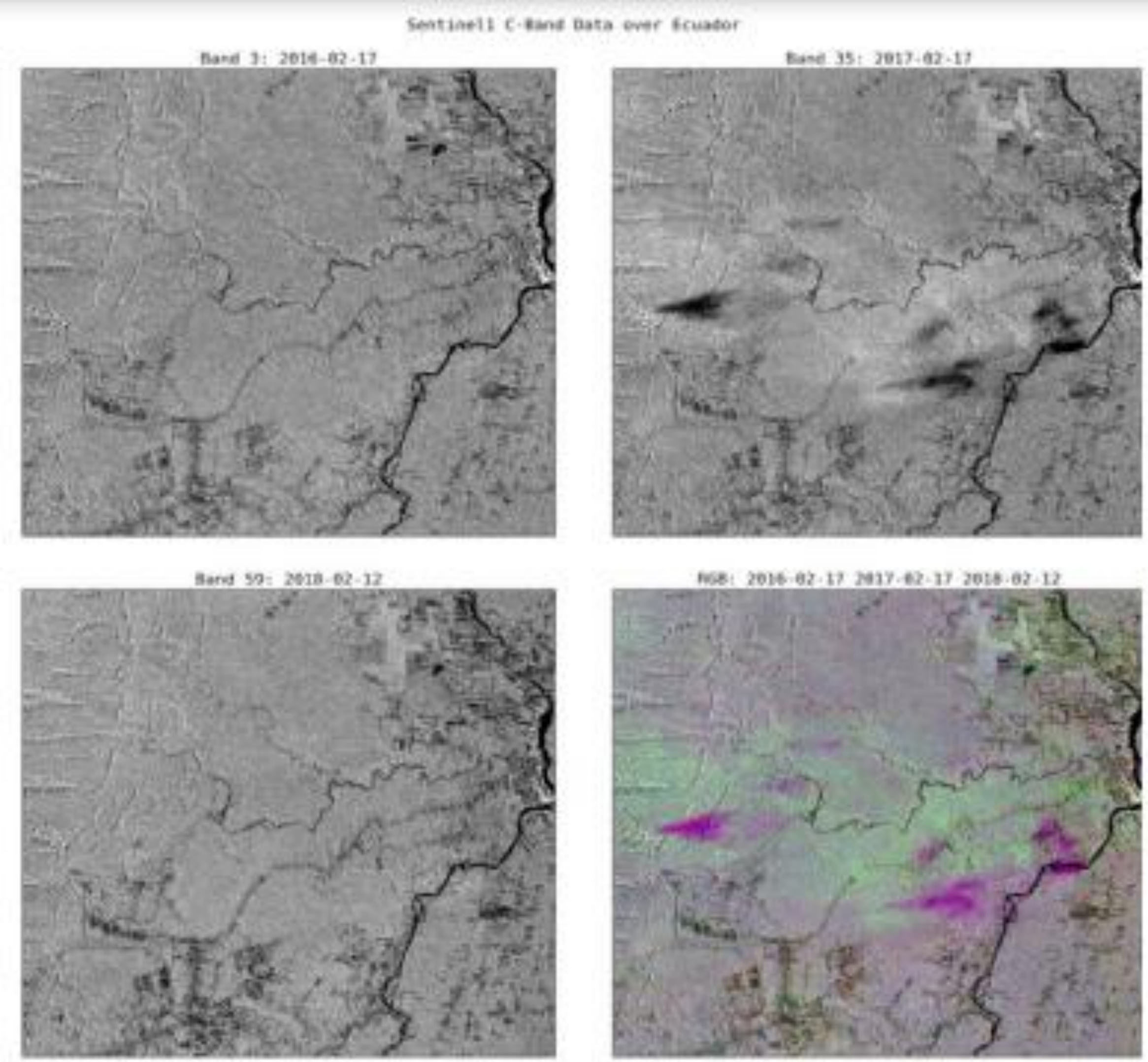

Sentinel-1 CVV example of moisture infuence on enhancing and darkening backscatter (Flores et al., 2019)

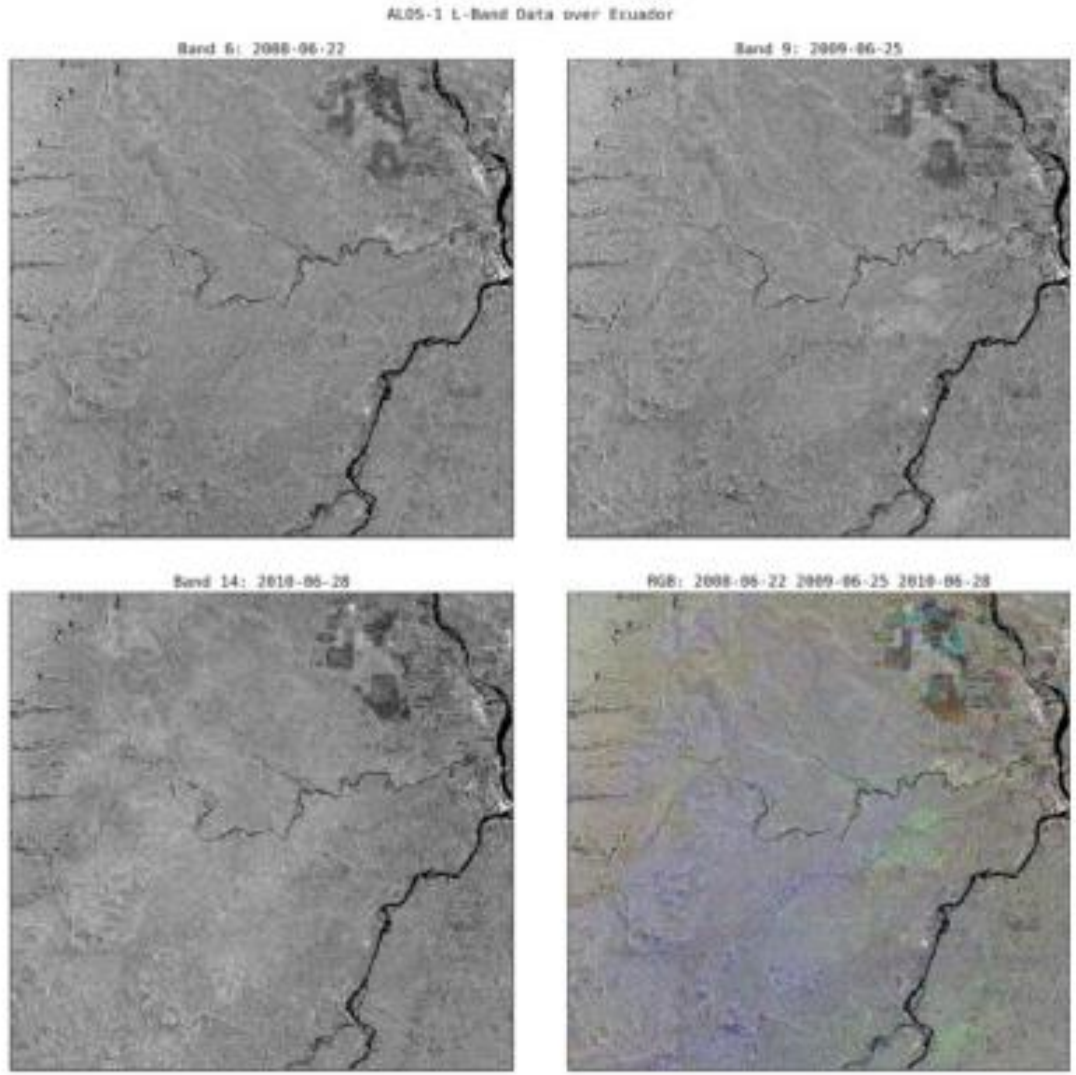

ALOS-1 L-HH example of moisture infuence on enhancing backscatter (Flores et al., 2019)

Effect of the presence of water under the canopy

- Double-bounce effect (Richards et al., 1987)

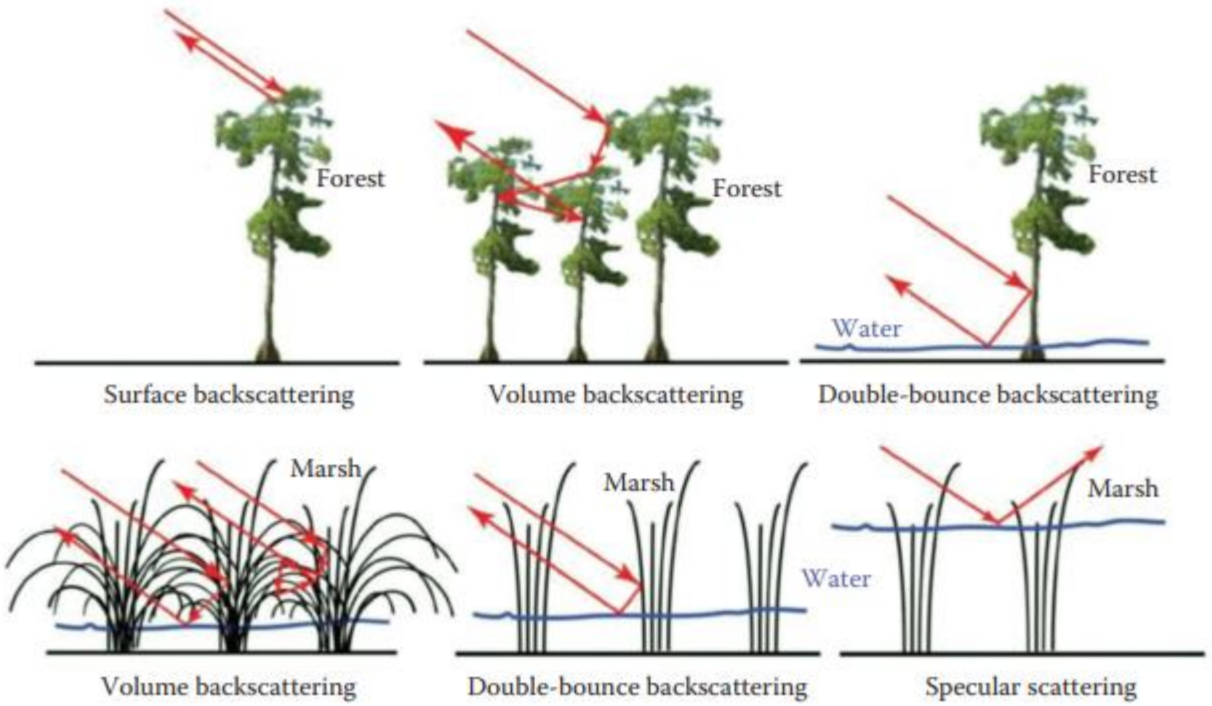

Schematic illustrating the different microwave scattering processes for forest and wetland vegetation (Brisco, 2015)

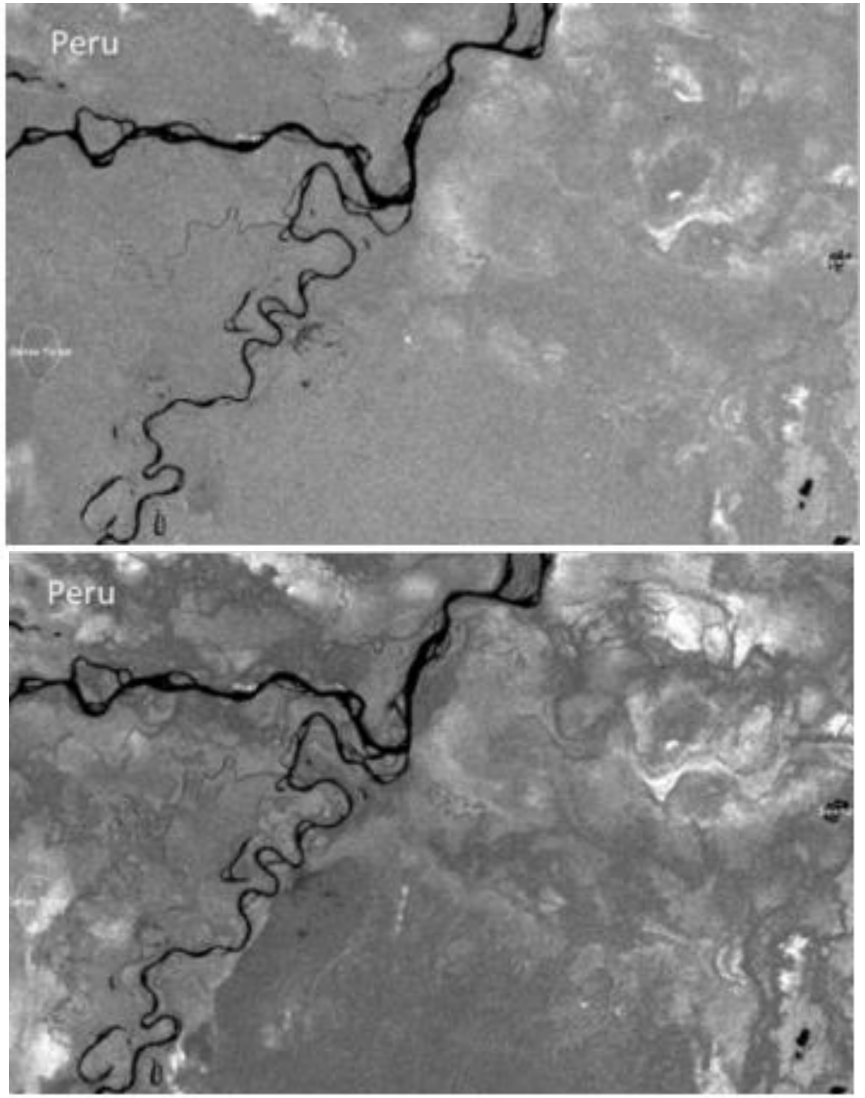

Double-bounce effect from bellow-canopy fooding at L-HH polarization from ALOS-1:
(top) Low-water season and (bottom) high-water season.

Forest stand height estimation

Relating SAR observations to forest stand height

❖ **Relating SAR to forest stand height**

- Increase of scatterers $\Rightarrow$ increase in power received (σ^0) moderated by signal attenuation by forest canopy.
  Empirical relationships between backscattering and forest height/biomass

The backscatter power, after correcting for topographic and other geometric effects, is written as

$$\gamma^0 = A\left(1-e^{-Bh_v^C}\right),$$

where γ^0 is the terrain-corrected form of radar cross section (e.g., see Small 2011), h_v is the vegetation height, and the coefficients A, B, and C are determined in the FSH algorithm using a least-squares fit between the backscatter power and the vegetation height provided by the ground validation and/or overlap data between scenes.

- SAR Interferometry (InSAR) height estimates (canopy) respectively to Digital Elevation Model (DEM) (ground)

- Merging with other types of Earth Observations (EO)
  e.g., lidar provides estimates of forest stand height as difference between first echo (top of canopy) and the echo corresponding to the ground

Empirical relationships between SAR/InSAR and forest height

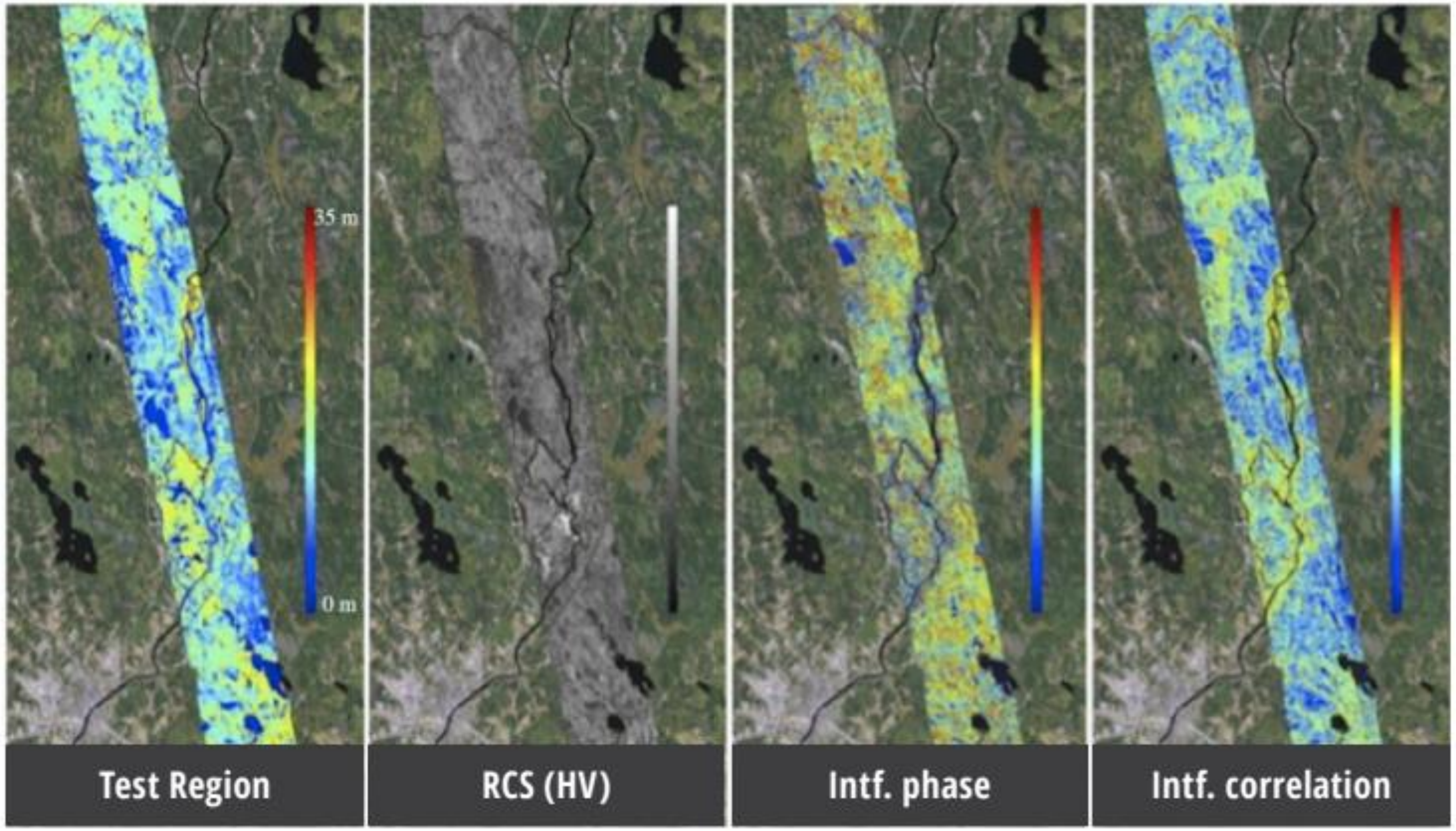

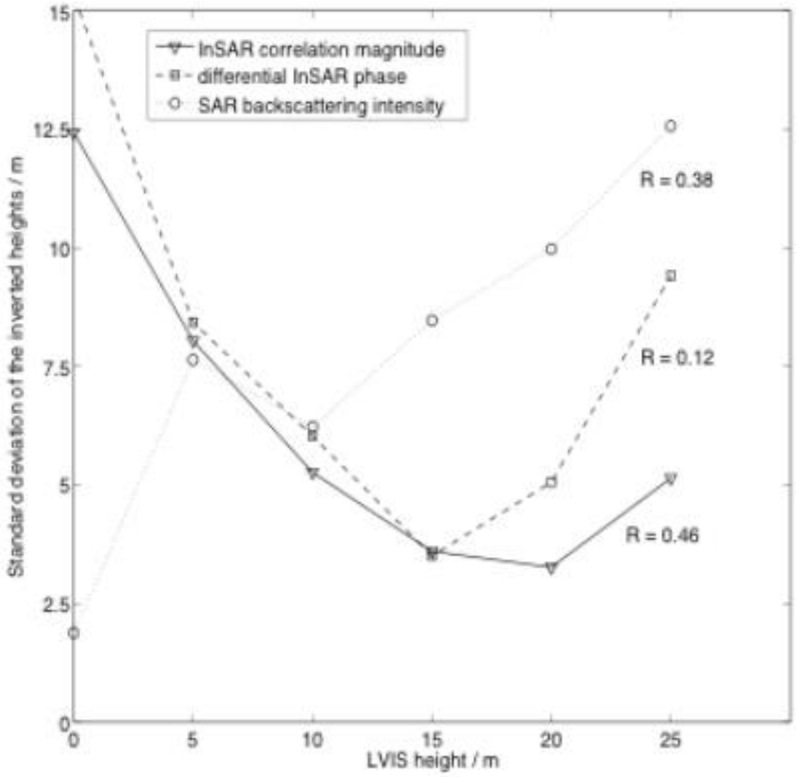

(a) a test region (Maine, USA) imaged by the LVIS lidar sensor, (b) the radar backscatter intensity (grayscale), (c) the height diference between L-band repeat-pass SAR and the ground surface DEM, and (d) a height estimate based on the interferometric correlation, (e) shows the FSH error relative to the lidar measurement for each of the three SAR methods derived from the cross-polarized signal. It can be seen from the plot that for vegetation heights of less than 10 m, the backscatter intensity is most accurate. For vegetation taller than 10 m, the InSAR coherence proves to be more accurate (Flores et al., 2019)

InSAR basic notions

❖ InSAR principle

Let’s consider to SAR images forming an interferogram

$$v(\cdot) = u_1(\cdot)u_2^*(\cdot) = |u_1(\cdot)\|u_2(\cdot)| \exp\{j\phi(\cdot)\} \qquad \text{where}$$

(Bamler and Hall, 1998)

$$\phi(\cdot) = \phi_1(\cdot) - \phi_2(\cdot)$$

$$\phi_1 = -2kR_1 + \phi_{\text{scat},1} \qquad \text{and} \qquad \phi_2 = -2kR_2 + \phi_{\text{scat},2}.$$

$$\phi = 2k\Delta R = \frac{4\pi}{\lambda}\Delta R.$$

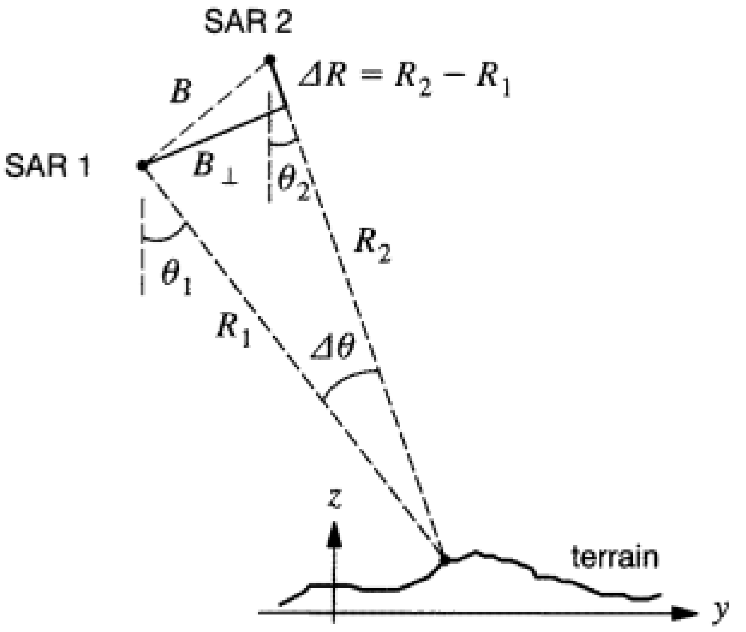

Across-track SAR interferometer (flight paths perpendicular into plane).

❖ Interferometric coherence

The local coherence estimator is the cross-correlation coefficient of the couple estimated on a small window:

$$\gamma = \frac{\langle E_1 E_2^* \rangle}{\sqrt{\langle |E_1|^2 \rangle \langle |E_2|^2 \rangle}},$$

$$\gamma = \gamma_{geom} \cdot \gamma_{SNR} \cdot \gamma_{vol} \cdot \gamma_{temp}$$

InSAR stand forest height estimates

❖ **Ground to volume power ratio (GVR) model (Treuhaft et al., 1996)**

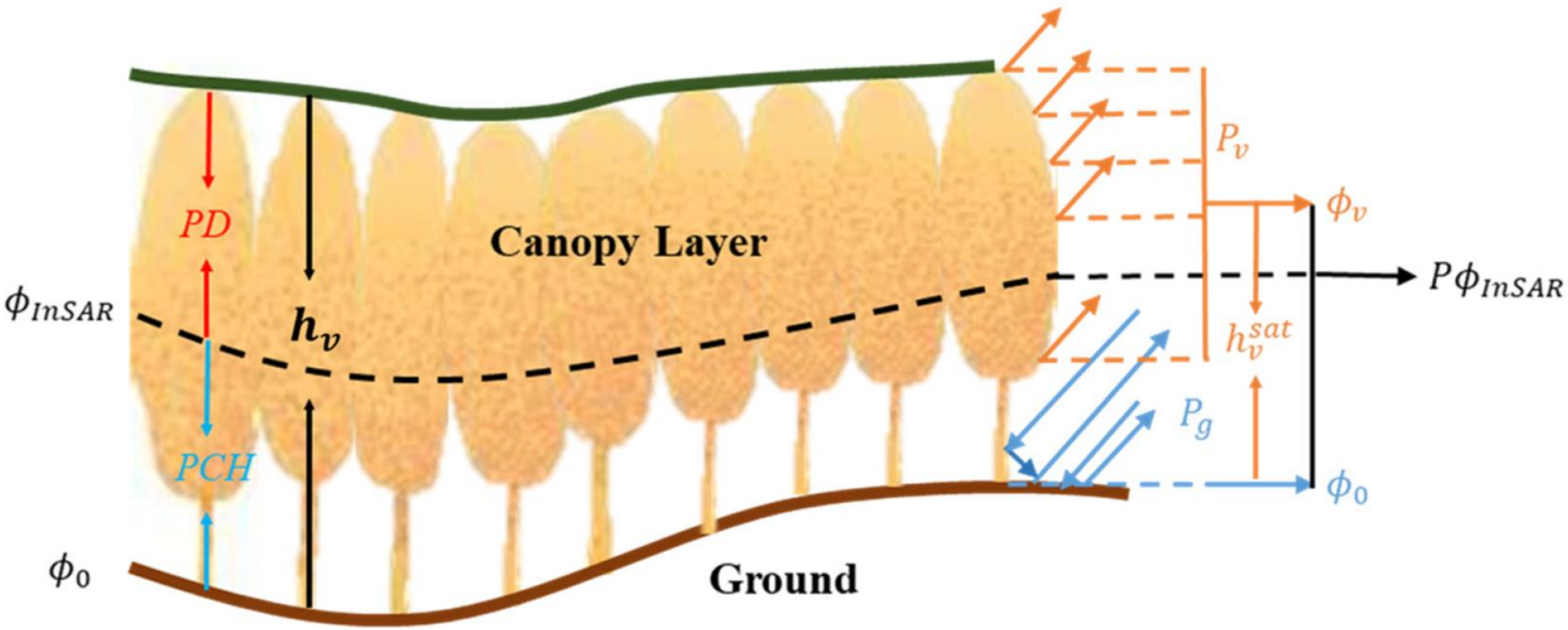

The saffron color denotes the volume scattering from the canopy layer, with phase center ϕ_v. The blue color represents the ground scattering, with phase center ϕ_0. The InSAR backscattered signal consists of the superposition of both; hence, with phase center ϕ_{InSAR}.

He et al. (2023)

InSAR stand forest height estimates

He et al. (2023)

InSAR coherence: $$\hat{\gamma} = e^{i\phi_0}\left(\hat{\gamma_v} + \frac{\mu}{1+\mu}\left(1 - \hat{\gamma_v}\right)\right)$$

where ϕ_0 is the ground phase; μ denotes the GVR; and $\hat{\gamma_v}$ represents the pure volume scattering coherence, which is given by

$$\hat{\gamma_v} = \frac{\int_0^{h_v} exp\left(\frac{2\sigma z}{cos\theta}\right) exp\left(ik_z z\right)dz}{\int_0^{h_v} exp\left(\frac{2\sigma z}{cos\theta}\right)dz}$$

where h_v is the canopy height; σ is the mean extinction coefficient; θ represents the local incidence angle; and k_z is the vertical wavenumber, which is expressed as

$$k_z = m\frac{2\pi B_\perp}{\lambda R \sin\theta}$$

where $B_\perp$ is the length of the perpendicular baseline, λ represents the wavelength, and R is the slant range. For bistatic acquisitions, $m = 1$, whereas for monostatic acquisitions, $m = 2$. In the absence of ground contribution, Equation (1) can be written as

$$\hat{\gamma} = e^{i\phi_0}\hat{\gamma_v}$$

InSAR stand forest height estimates

$$\phi_{InSAR} = tan^{-1}\frac{sin(k_z\frac{PD(1+\mu)}{\mu}+\phi_0)+\mu\, sin\,\phi_0}{cos(k_z\frac{PD(1+\mu)}{\mu}+\phi_0)+\mu\, cos\,\phi_0}$$

He et al. (2023)

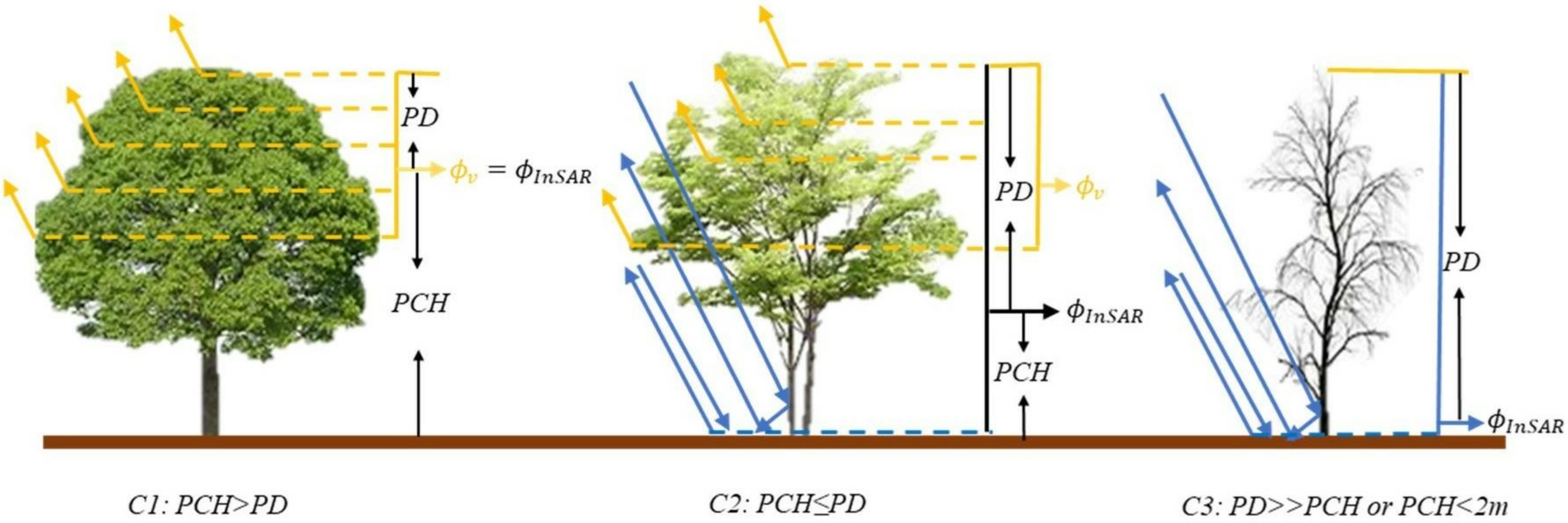

Multi-satellite stand forest height estimates

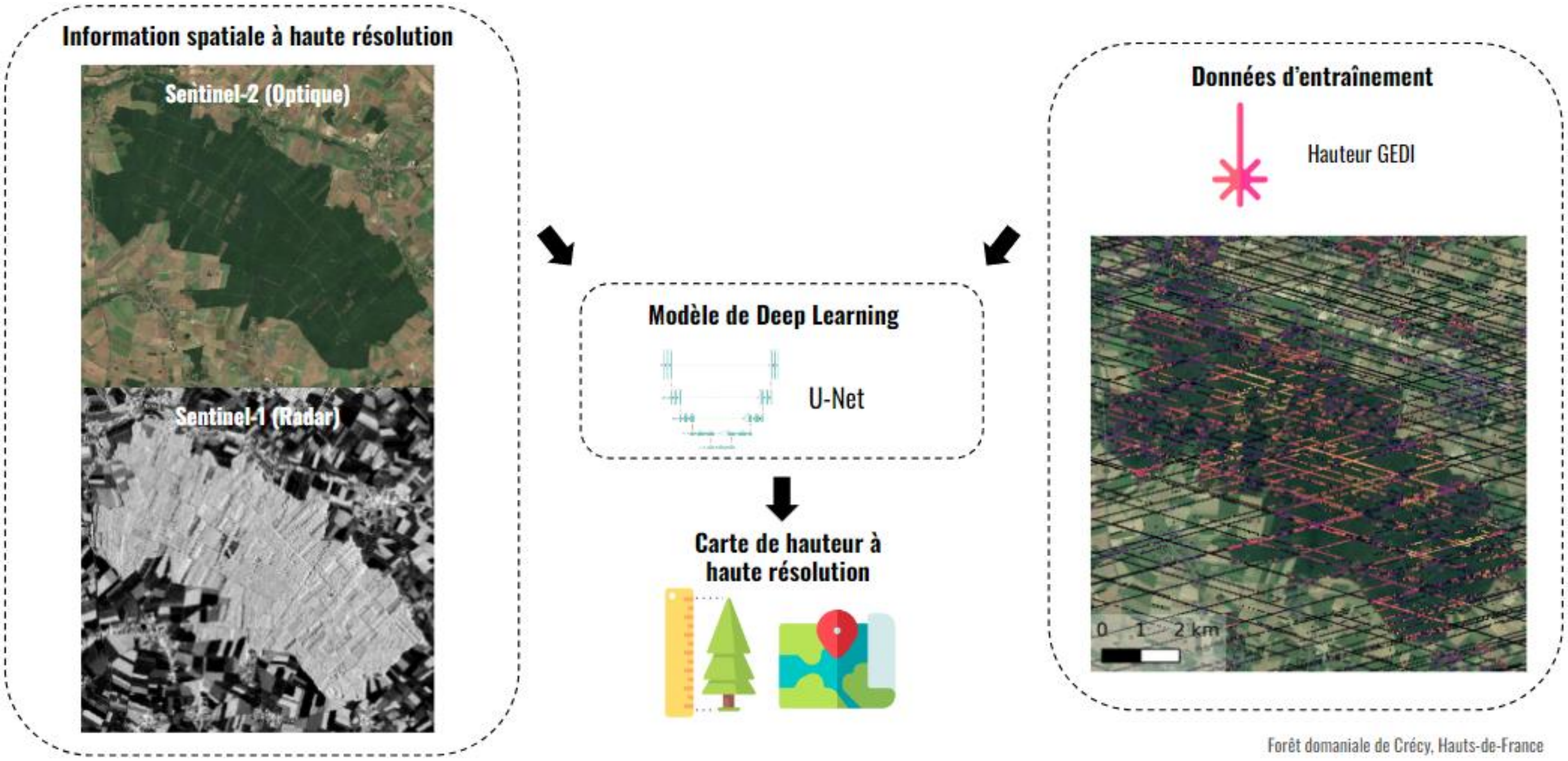

Multi-satellite stand forest height estimates

- Permet d'extraire la **texture** et le **contexte** de l'image à **plusieurs échelles**

- ~ **17 Millions** de paramètres à ajuster

- Particulièrement adapté aux **gros jeux de données** (GEDI)

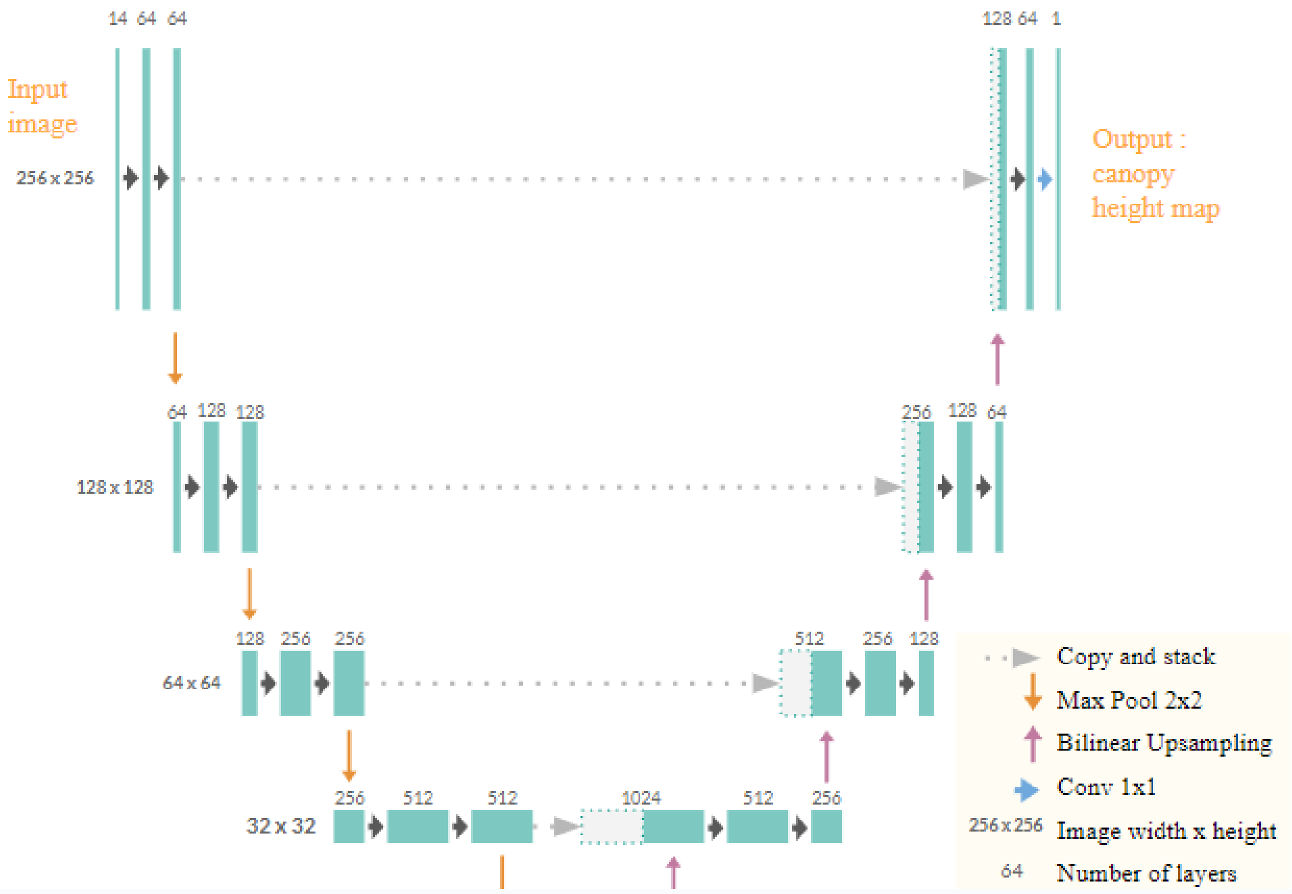

Multi-satellite stand forest height estimates

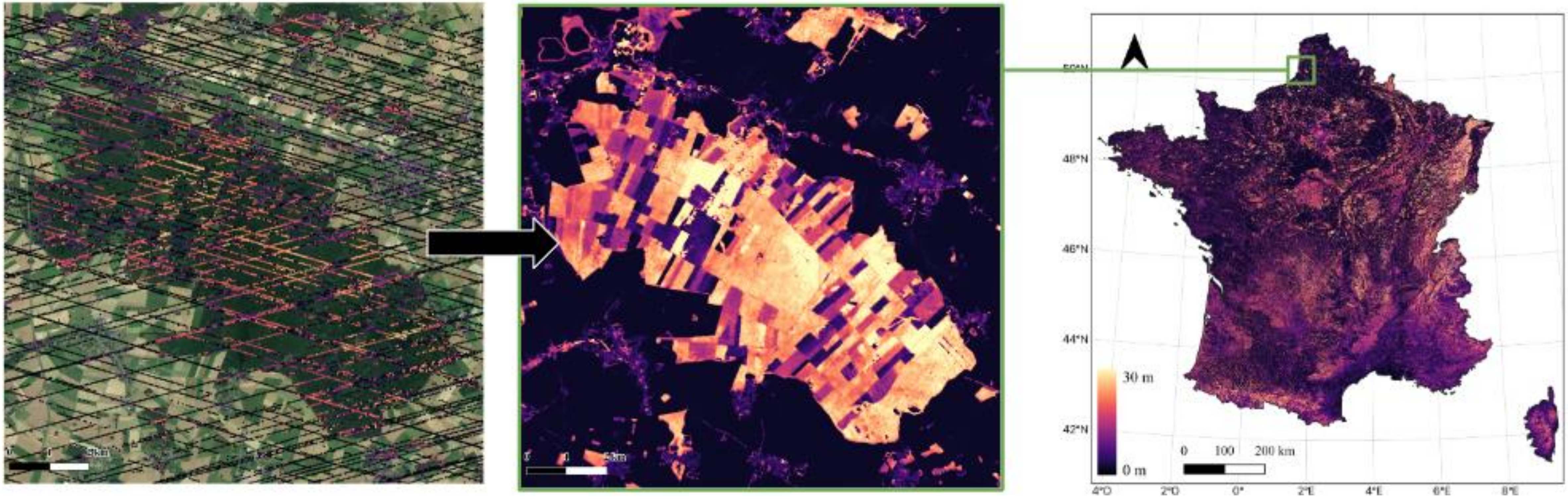

Schwartz et al., (2023)

Multi-satellite stand forest height estimates

Passage hauteur -> volume et biomasse par relations allométriques

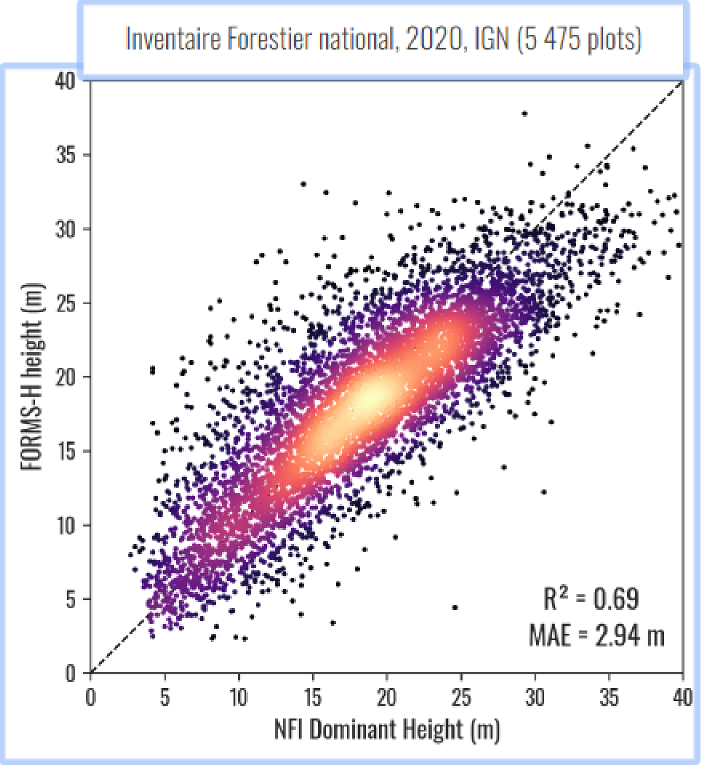

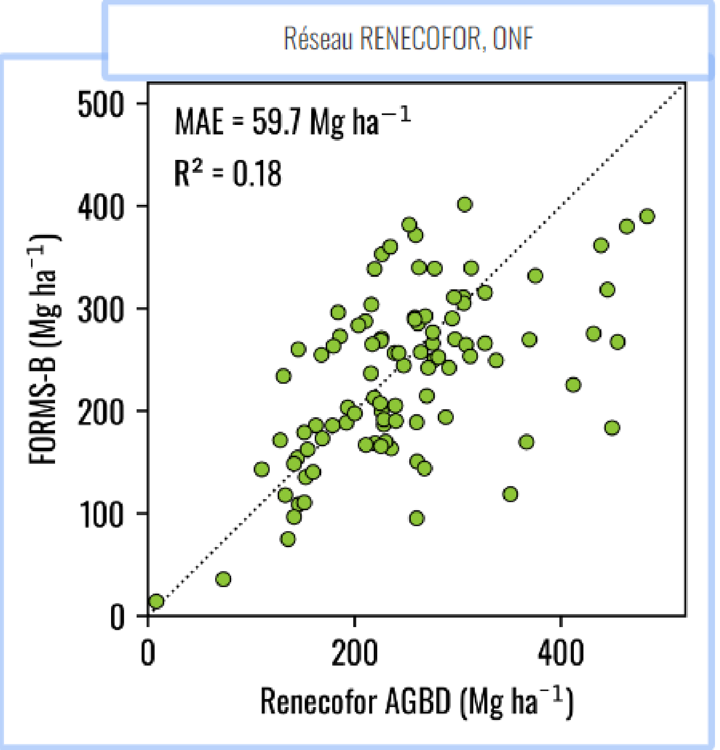

Schwartz et al., (2023)